Supporting information for

Revisiting water sorption isotherm of MOF using electrical measurements

Shyamapada Nandi,[a] Himanshu Aggarwal,[b,c] Mohammad Wahiduzzaman,[a] Youssef Belmabkhout,[b] Guillaume Maurin,[a] Mohamed Eddaoudi,[b] Sabine Devautour-Vinot[a]

[a]Institut Charles Gerhardt Montpellier, UMR 5253 CNRS, UM, ENSCM Université Montpellier, Place E. Bataillon, 34095 Montpellier cedex 5, France.

[b]King Abdullah University of Science and Technology, Division of Physical Sciences and Engineering, Advanced Membranes & Porous Materials Center, Functional Materials Design, Discovery & Development Research Group, Thuwal 23955-6900, Kingdom of Saudi Arabia

[c]Birla Institute of Technology and Science-Pilani, Hyderabad Campus, Jawahar Nagar, Shamirpet, Hyderabad, India.

1. Synthesis

All the chemicals were bought from Sigma Aldrich and used without further purification.

Synthesis of Cr-soc-MOF-1:

A solution of $FeCl_3 \cdot 6H_2O$ in DMF (0.1 M, 0.3 mL, 0.03 mmol) was prepared and added to a mixture of H_4TCPT (7.1 mg, 0.01 mmol), DMF (1 mL), and acetonitrile (1 mL) in a 20 mL scintillation vial. A dilute nitric acid solution in DMF (3.5 M, 1.5 mL) was prepared separately and added to the reaction mixture. The clear orange-yellow solution was then placed in a preheated oven at 115 °C for 3 days to obtain square block shaped orange-yellow shaped. The crystals were subsequently washed with fresh DMF and the DMF was replaced every 4-5 hours. After washing the crystals with DMF for 24 hours, the crystals were immersed in acetone and thrice daily over a period of 3 days.[1] The sample was activated by heating at 393 K for 8 hrs under dynamic vacuum.

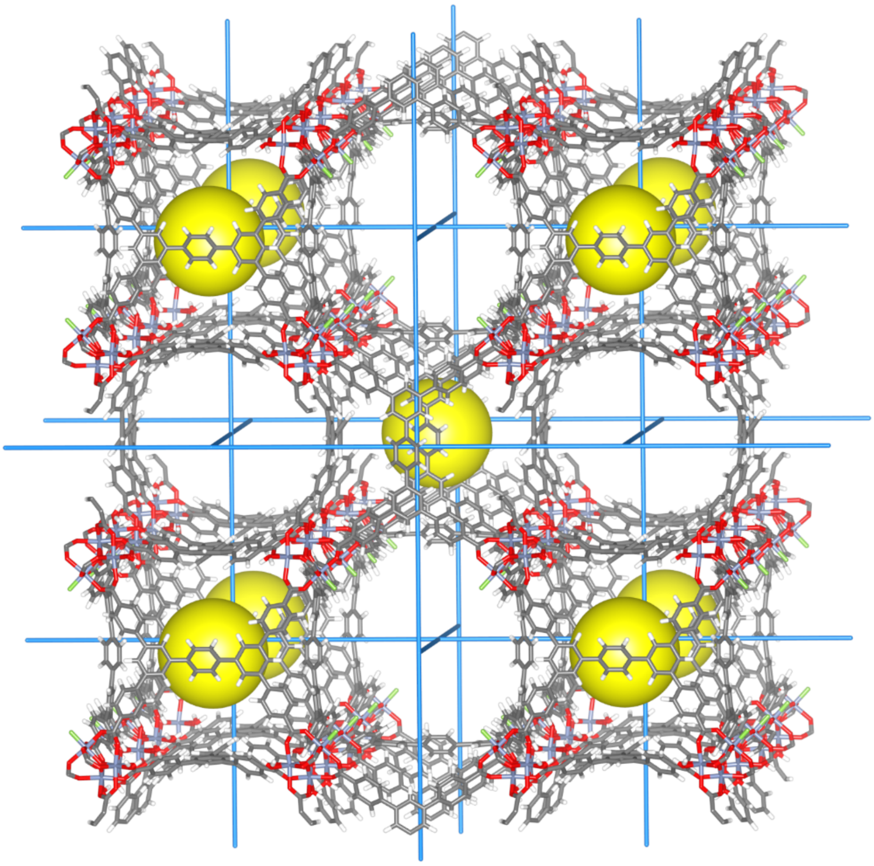

Figure S1. Schematic representation of in Cr-soc-MOF-1 in which yellow spheres are representing the cubic cages and the blue lines are showing the interconnected channels. Color code: C, gray; O, red; Cl, green; Cr, blue, H, white.

2. X-Ray Powder Diffraction data

Powder XRD patterns of the solids before and after conductivity measurements were collected on a PANalytical X'Pert equipped with an X'Celerator detector and using a wavelength, λ =1.5406 Å with an operating voltage of 40 kV and a beam current of 30 mA.

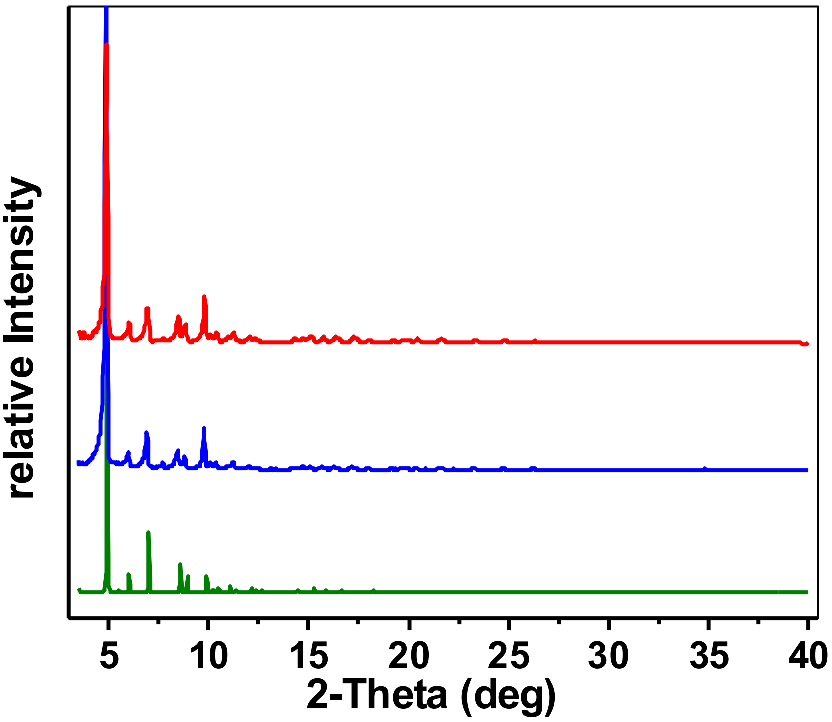

Figure S2. Simulated (green) and experimental XRPD patterns of Cr-soc-MOF-1 before (red) and after (blue) impedance measurements.

3. N_2 Adsorption Isotherm

N_2 adsorption isotherms were collected on the activated solid at 77 K using a Quadrasorb evo - Quantachrome Instrument.

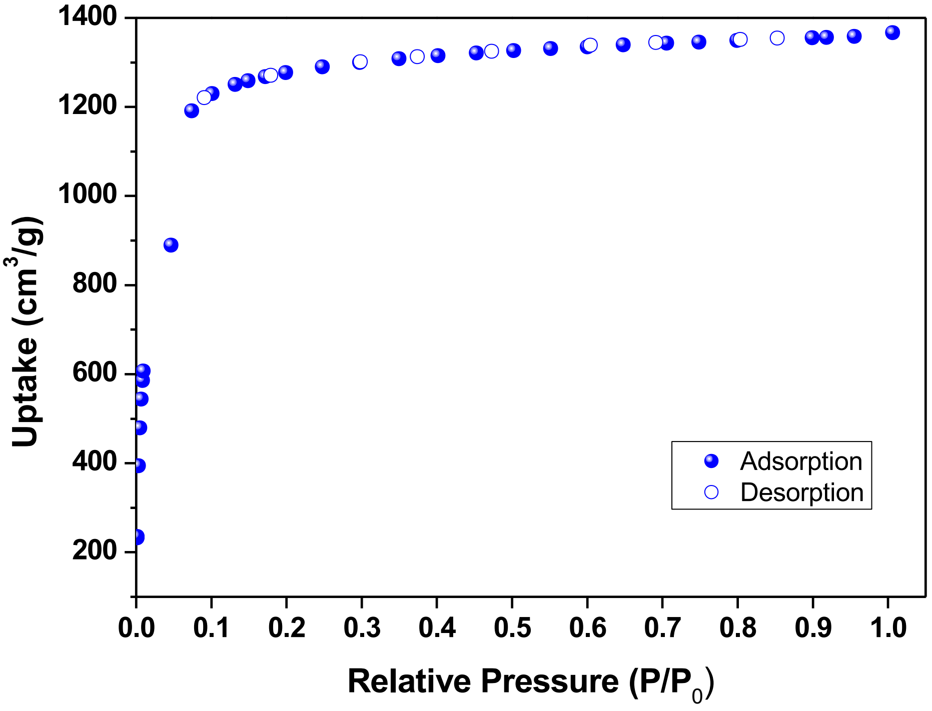

Figure S3. N_2 sorption isotherm of Cr-soc-MOF1 recorded at 77 K.

The corresponding pore volume is 2.1 $cm^3.g^{-1}$ and the BET area is 4540 $m^2.g^{-1}$, which matches very well with the previously reported data[1], as well as with the calculated values deduced from the fully geo-optimized solid (cf modelling part: $V_{pore\ volume}$ = 2.1 $cm^3.g^{-1}$ and S_{BET} = 4665 $m^2.g^{-1}$).

4. Conductivity

The humidity dependant impedance measurements were carried out using a solartron (Ametek) impedance analyzer over a frequency range from 1Hz to 1 MHz with an applied voltage of 1 V. The powder sample of Cr-soc-MOF-1 was placed between two gold electrodes in a parallel plate capacitor configuration with an annular Teflon spacer to provide insulation, allowing the use of the "two-probe" method for the electrical measurements. The relative humidity and temperature were controlled by a 'Bench-Top Type Temperature and Humidity Chamber' form ESPEC Corporation. It is composed by a small liquid water "bath" located in the mixing plenum; as the chamber air is drawn into the plenum, it passes the bath, picking up vapor submitted to the sample. To establish the electrical isotherms, impedance data were recorded upon increasing (adsorption) and decreasing (desorption) the Relative Humidity (RH) at 298 K and 363 K. The sample was equilibrated for at least 12 hours, before changing the RH/T conditions, even the equilibration time can be shortened to 1.5 hour, as evidenced in Figure S4.

The resistance R of the solids was deduced from the analysis of the Nyquist plots (-Z" = f(Z')), that is from the semi-circle extrapolation to the real-axis, while the corresponding conductivity values σ were obtained using $\sigma = 1/R \times l/S$, where l and S are the sample thickness and area respectively.

In the Bode representation ($\sigma'_{ac} = f(F)$), the real part of the ac conductivity, σ'_{ac} (ω,T), usually results from the combination of three contributions: $\sigma'_{ac}(\omega,T) = \sigma'_{MWS}(\omega,T) + \sigma_{dc}(T) + \sigma'(\omega,T)$. The polarization component $\sigma'(\omega,T)$, corresponding to the increasing part of the signal, arises from the local rearrangement of charges or dipoles causing dipolar reorientation. The dc conductivity plateau σ_{dc} (T) results from the long-range redistribution of charges. In case of highly conductive materials, the Maxwell Wagner Sillars contribution σ'_{MWS} (ω,T) due to the charge accumulation to the sample/electrode interface is observed at low frequency. The absence of the dc plateau in the Bode representation for the anhydrous solid relates with the insulating behaviour of Cr-soc-MOF-1 in the whole domain of explored temperatures and further evidence that a guest mediator is required to allow the proton transfer throughout the porosity of the solid.

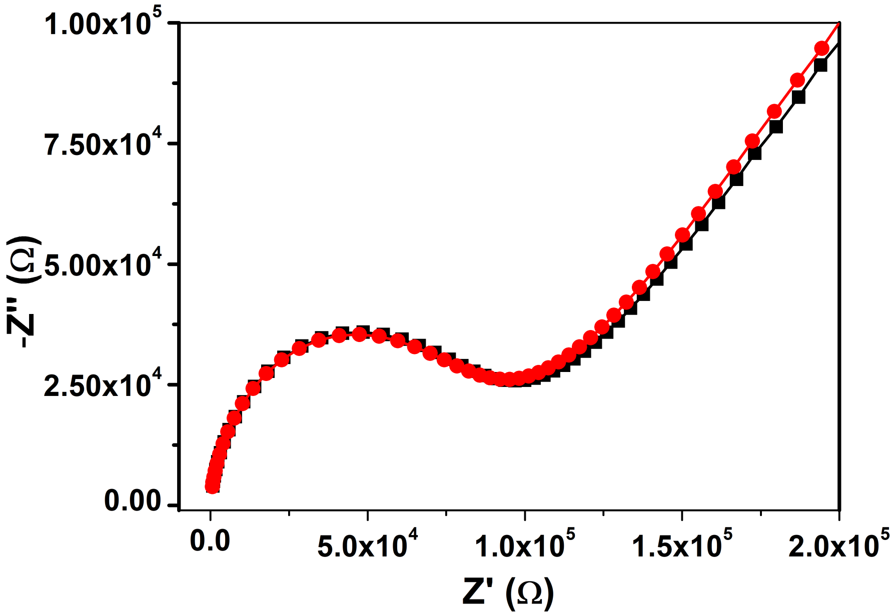

Figure S4. Nyquist plot from ac impedance data for the Cr-soc-MOF-1 recorded at 363 K under 70% RH after 12 (black) and 24 (red) hours of equilibration.

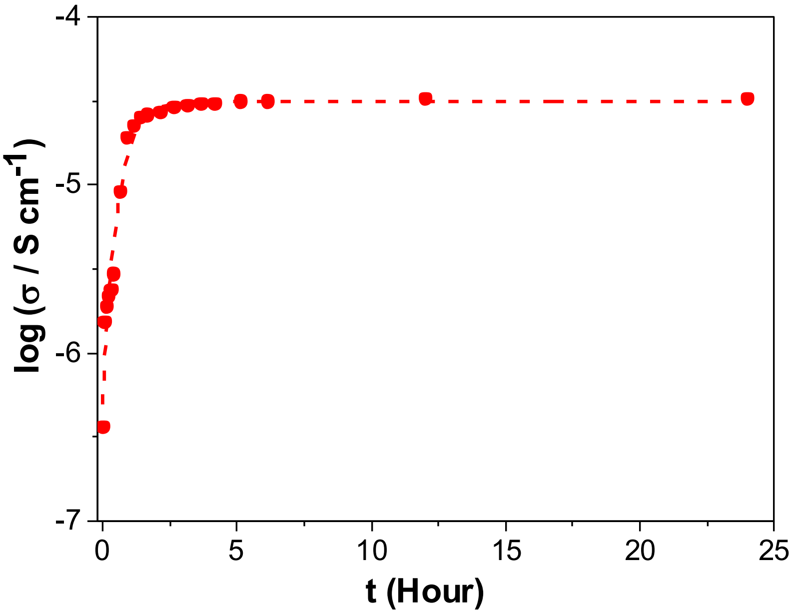

Figure S5. Time evolution of the conductivity of Cr-soc-MOF-1 recorded at 363 K under 70% RH. The conductivity recorded at 90°C/70%RH converges towards a steadily value for 1,5 hrs of equilibrium.

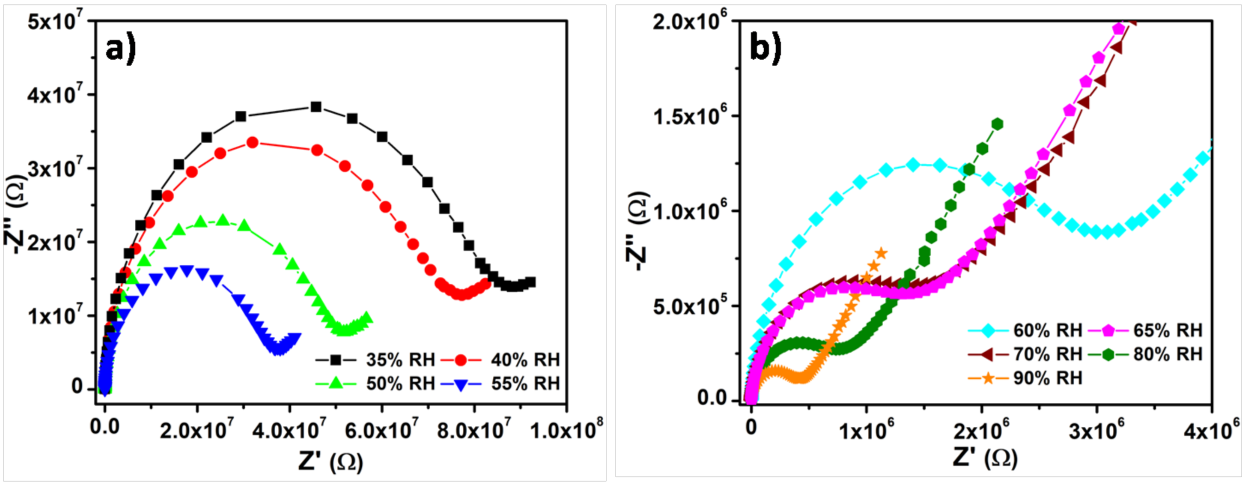

Figure S6. Nyquist plots from ac impedance data for the Cr-soc-MOF-1 recorded at 298 K under (**a**) 35% RH (black), 40% RH (red), 50% RH (green), 55% RH (blue) and (**b**) 60% RH (cyan), 65% RH (magenta), 70% RH (wine), 80% RH (olive) and 90% RH (orange) upon increasing RH.

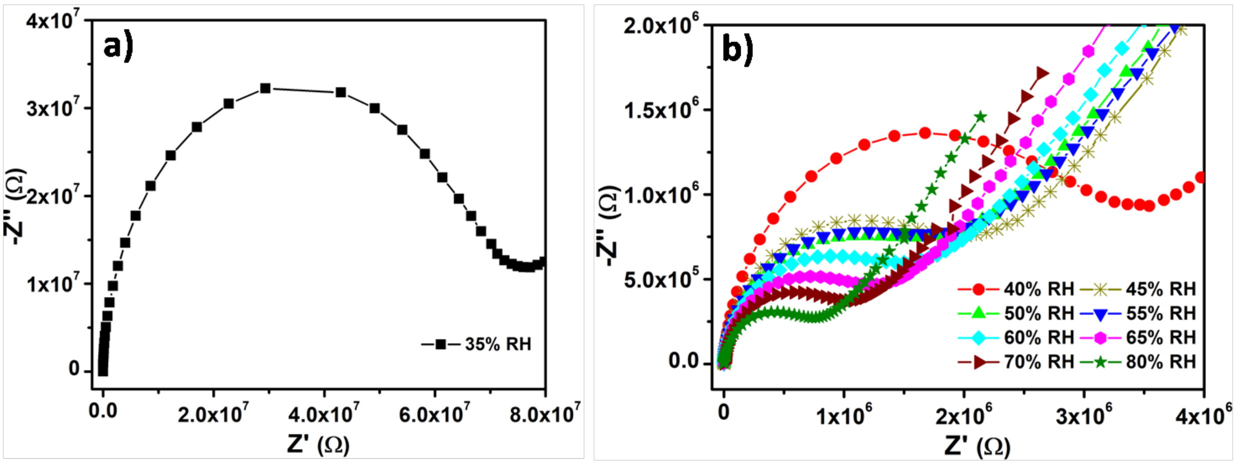

Figure S7. Nyquist plots from ac impedance data for the Cr-soc-MOF-1 recorded at 298 K under (**a**) 35% RH and (**b**) 80% RH (olive), 70% RH (wine), 65% RH (magenta), 60% RH (cyan), 55% RH (blue), 50% RH (green), 45% RH (dark yellow) and 40% RH (red) upon decreasing RH.

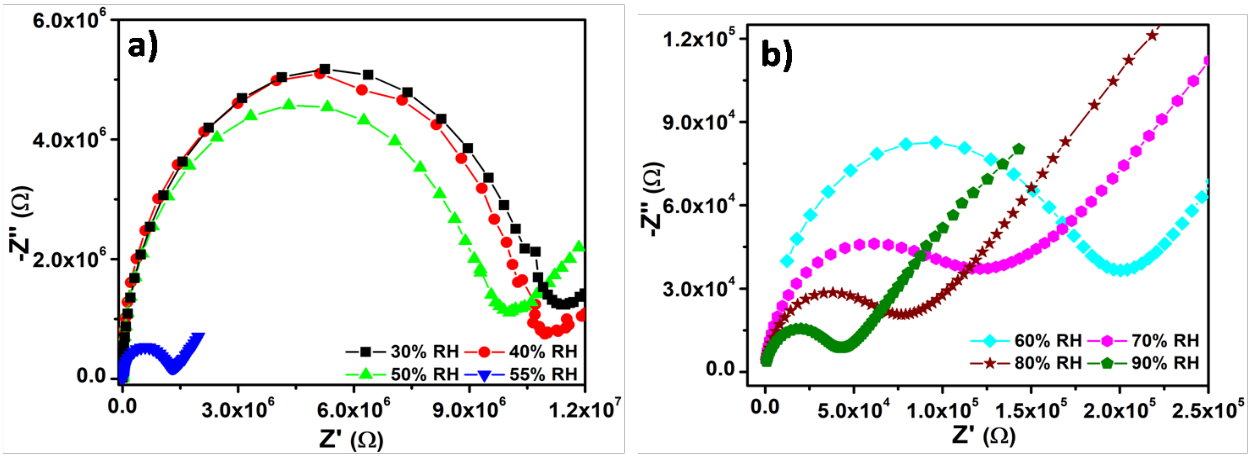

Figure S8. Nyquist plots from ac impedance data for the Cr-soc-MOF-1 recorded at 363 K under (**a**) 30% RH (black), 40% RH (red), 50% RH (green) 55% RH (blue) and (**b**) 60% RH (cyan), 70% RH (magenta), 80% RH (wine) and 90% RH (olive) upon increasing RH.

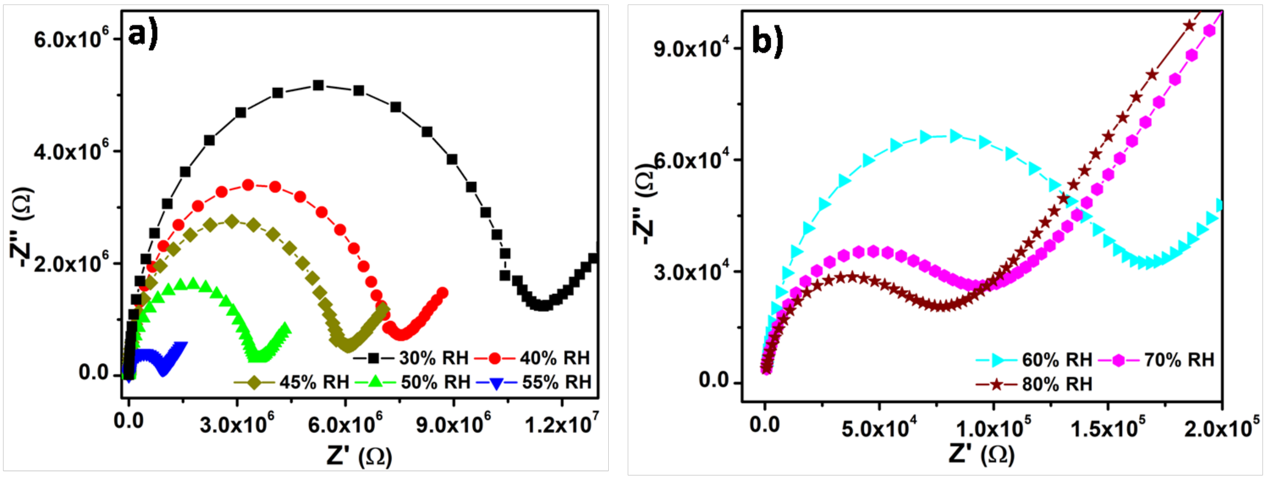

Figure S9. Nyquist plots from ac impedance data for the Cr-soc-MOF-1 recorded at 363 K under (**a**) 30% RH (black), 40% RH (red), 45% RH (dark yellow), 50% RH (green), 55% RH (blue) and (**b**) 60% RH (cyan), 70% RH (magenta) and 80% RH (wine) upon decreasing RH.

Table S1. Conductivity values recorded at 298 K and 363 K for the Cr-soc-MOF-1 upon increasing and decreasing RH.

Adsorption branch T = 298 K		**Desorption branch T = 298 K**	
RH %	**σ Scm^{-1}**	**RH %**	**σ Scm^{-1}**
35	2.4×10^{-8}	**35**	2.7×10^{-8}
40	2.7×10^{-8}	**40**	6.1×10^{-7}
50	4.0×10^{-8}	**45**	9.7×10^{-7}
55	5.7×10^{-8}	**50**	1.1×10^{-6}
60	7.0×10^{-7}	**55**	1.2×10^{-6}
65	1.6×10^{-6}	**60**	1.5×10^{-6}
70	1.6×10^{-6}	**65**	1.6×10^{-6}
80	2.6×10^{-6}	**70**	2.0×10^{-6}
90	5.1×10^{-6}	**80**	3.3×10^{-6}
Adsorption branch T = 363 K		**Desorption branch T = 363 K**	
30	1.8×10^{-7}	**30**	1.8×10^{-7}
40	1.9×10^{-7}	**40**	2.8×10^{-7}
50	2.1×10^{-7}	**45**	3.5×10^{-7}
55	1.6×10^{-6}	**50**	5.9×10^{-7}
60	1.0×10^{-5}	**55**	2.2×10^{-6}
70	1.7×10^{-5}	**60**	1.2×10^{-5}
80	2.8×10^{-5}	**70**	2.2×10^{-5}
90	5.0×10^{-5}	**80**	2.8×10^{-5}

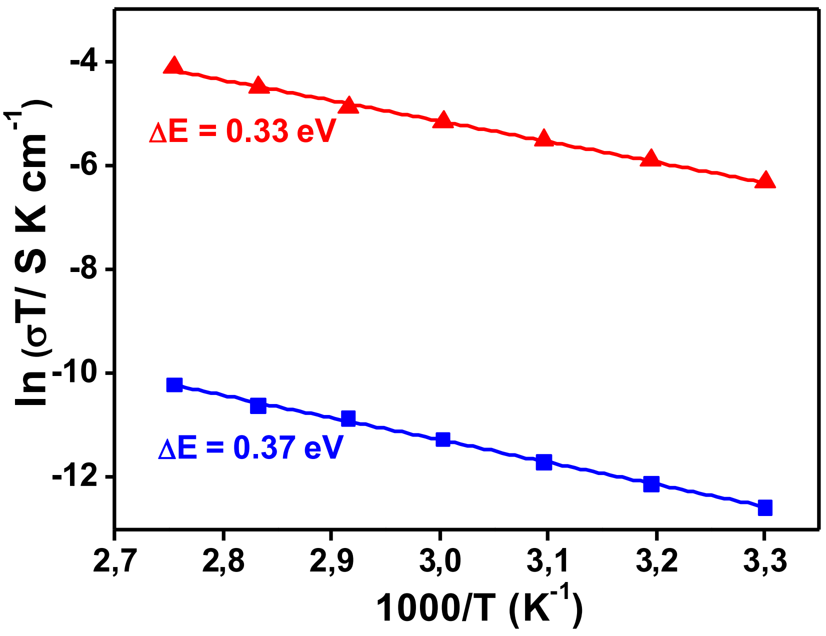

Figure S10. Arrhenius plot of the conductivity for Cr-soc-MOF-1 under 40% RH (blue square) and 80% (red triangle) of RH. The lines correspond to the linear least-square fit.

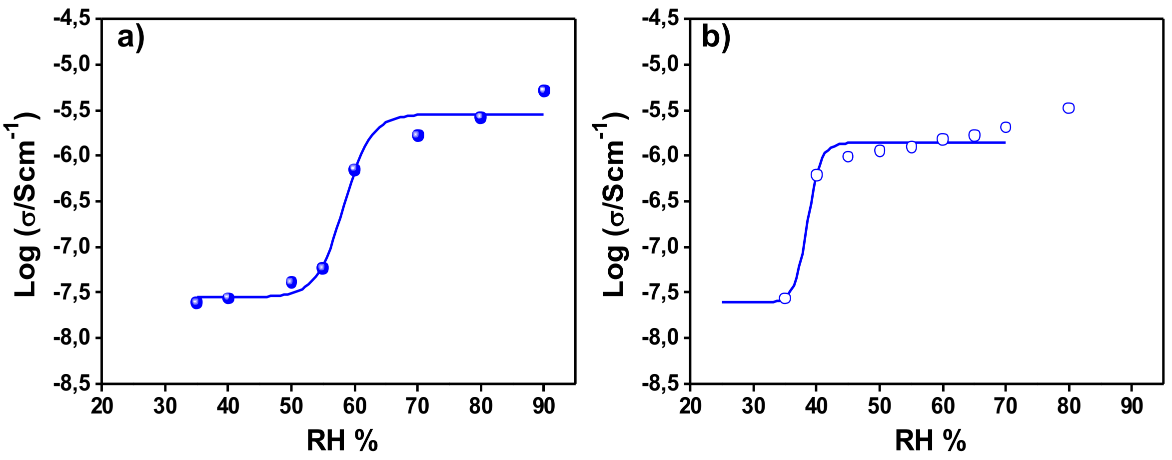

Figure S11. Sigmoidal curve fitting (solid line) of the "electrical" water adsorption (**a**-solid spheres) and desorption (**b**-empty circles) isotherms for Cr-soc-MOF-1 at 298 K obtained by impedance spectroscopy.

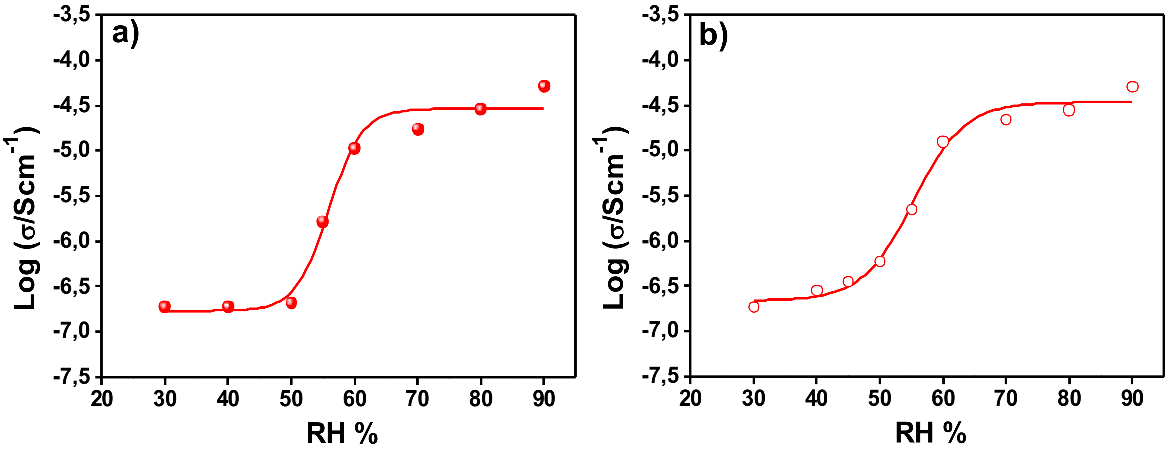

Figure S12. Sigmoidal curve fitting (solid line) of the "electrical" water adsorption (**a**-solid spheres) and desorption (**b**-empty circles) isotherms for Cr-soc-MOF-1 at 363 K obtained by impedance spectroscopy.

Table S2. α parameters deduced from the adsorption and desorption branches for the volumetric and electrical isotherms. α corresponds to the RH value at which half of the total water capacity is achieved.

Adsorption Isotherm	T (K)	α (adsorption branch)	α (desorption branch)
Volumetric Measurements	298	61	52
	363	65	62
Electrical Measurements	298	58	38
	363	56	55

5. Water Sorption Isotherm

The as-synthesized Cr-**soc**-MOF-1 crystals were treated with volatile solvents and heated prior to water vapor sorption experiments. As a common strategy crystals were exchanged acetone for 4-5 days, during which time the solvent was replaced 3-4 times per day. The crystals were then dried by heating under vacuum at 393 K or 8 h to yield activated samples. Temperature was increased to desire value from room temperature at the rate of 1 K min^{-1}. Activated sample was used for corresponding isotherm measurement. Sorption data was processed by using Helmholtz equation. The adsorption isotherms were recorded at three different temperatures 298 K and 363 K.

A volumetric apparatus Vstar1 vapor sorption analyzer from Quantachrome instruments was used for collecting water adsorption isotherms at different temperatures. Schematic diagram of the instrument is shown in the scheme S1, from the screenshot of the software window.

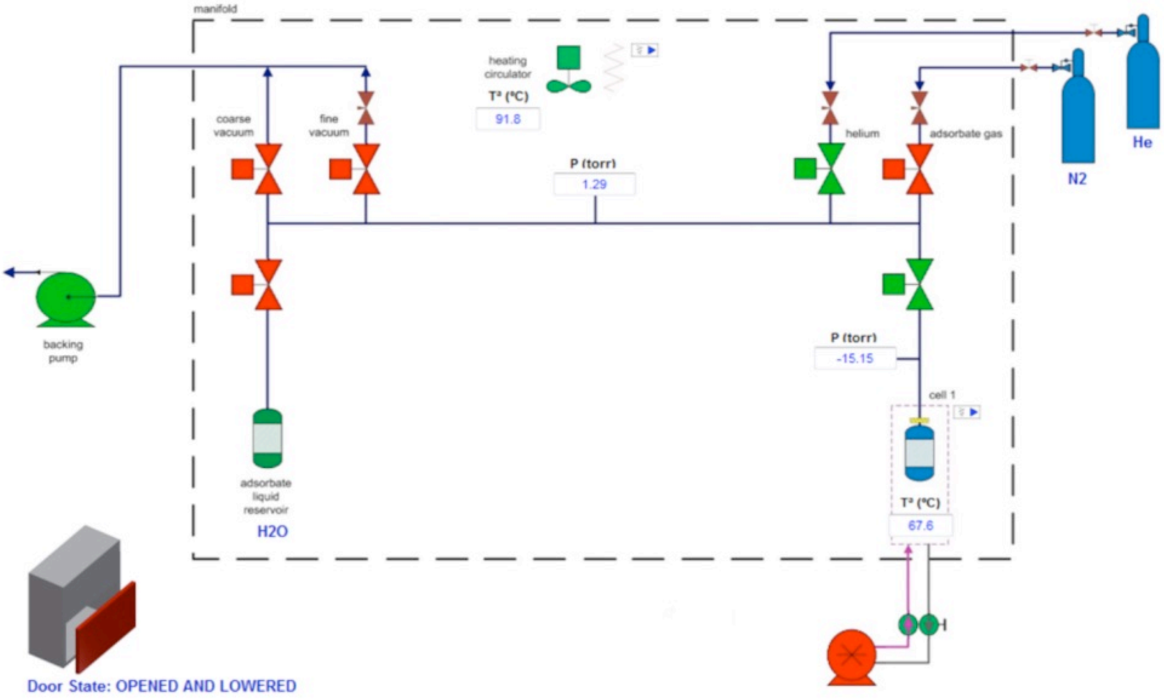

Scheme S1. Schematic representation of V-Star vapor sorption instrument.

6. Modelling

DFT calculations

The atomic positions of the Cr-soc-MOF-1 structure model that have been determined by single crystal diffraction data were further optimized with Kohn-Sham density-functional theory (DFT)[2,3] retaining the indexed cell parameters. This model includes two coordinated water molecules per Cr-oxo trimer (Ocw and Hcw being the labels of the corresponding water molecules) while the third Cr atom is bounded to a counter-anion, e.g. an F-atom in our case (see Figure S11).

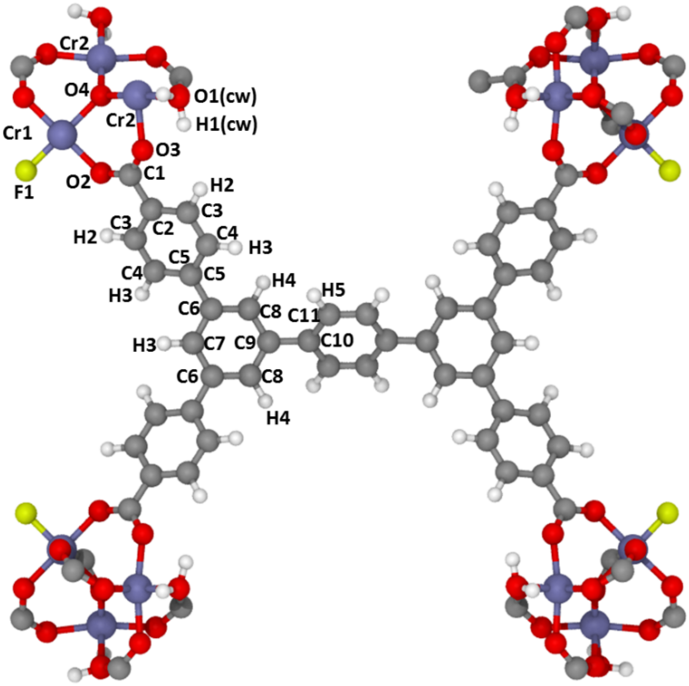

Figure S13. A representative portion of the Cr-soc-MOF-1 crystal structure showing the atom types in which the DFT-derived RESP charges were assigned.

DFT geometry optimization of this Cr-soc-MOF-1 model was performed using the Quickstep module[4] of the CP2K program[5,6] employing the Gaussian Plane Wave (GPW) formalism. The general gradient approximation (GGA) to the exchange-correlation functional according to Perdew-Burke-Ernzerhof (PBE)[7] in a combination of Grimme's DFTD3 semi-empirical dispersion corrections.[8,9] Triple-ζ plus valence polarized Gaussian-type basis sets (TZVP-MOLOPT) were considered for all atoms, except for the Cr centres, where short ranged double-ζ plus valence polarization functions (DZVP-MOLOPT) were employed.[10] The interaction between core electrons and valence shells of the atoms were described by the pseudopotentials derived by Goedecker, Teter, and Hutter (GTH).[11–13] The auxiliary plane wave basis sets were truncated at 400 Ry. In addition, single point energy calculation was performed to extract the atomic partial charges of Cr-soc-MOF-1 crystal applying the REPEAT fitting method[14] for the periodic system as implemented in the CP2K code.

Table S3: LJ potential parameters and partial charges of the atom types of Cr-soc-MOF-1 crystal structure.

	Atom Type	ε/k_B [K]	σ [Å]	q (e^-)
1	**H1(Hcw)**	0.0000	2.8460	0.377
2	**H2**	7.6490	2.8460	0.178
3	**H3**	7.6490	2.8460	0.130
4	**H4**	7.6490	2.8460	0.105
5	**H5**	7.6490	2.8460	0.121
6	**H6**	7.6490	2.8460	0.135
7	**C1**	47.8570	3.4730	0.593
8	**C2**	47.8570	3.4730	0.098
9	**C3**	47.8570	3.4730	-0.232
10	**C4**	47.8570	3.4730	-0.149
11	**C5**	47.8570	3.4730	0.144
12	**C6**	47.8570	3.4730	-0.036
13	**C7**	47.8570	3.4730	-0.105
14	**C8**	47.8570	3.4730	-0.151
15	**C9**	47.8570	3.4730	0.026
16	**C10**	47.8570	3.4730	0.106
17	**C11**	47.8570	3.4730	-0.175
18	**O1(Ocw)**	30.1940	3.1180	-0.719
19	**O2**	30.1940	3.1180	-0.553
20	**O3**	30.1940	3.1180	-0.632
21	**O4**	30.1940	3.1180	-1.081
22	**F1**	36.4830	3.0930	-0.532
23	**Cr1**	7.5480	2.6930	1.479
24	**Cr2**	7.5480	2.6930	1.719

Pore size distribution (PSD):

The geometric methodology reported by Gelb and Gubbins[15] was used to calculate the pore size distributions (PSD) of the geometry optimized structures, as depicted in Figure S12. In this calculation, the van der Waals parameters of the framework atoms were adopted from Universal Force Field (UFF).[16] It is shown that this MOF shows at least two distinct distribution peaks at ~11.5 Å and ~15 Å associated to the cubic cages formed by surrounded larger pore channel.

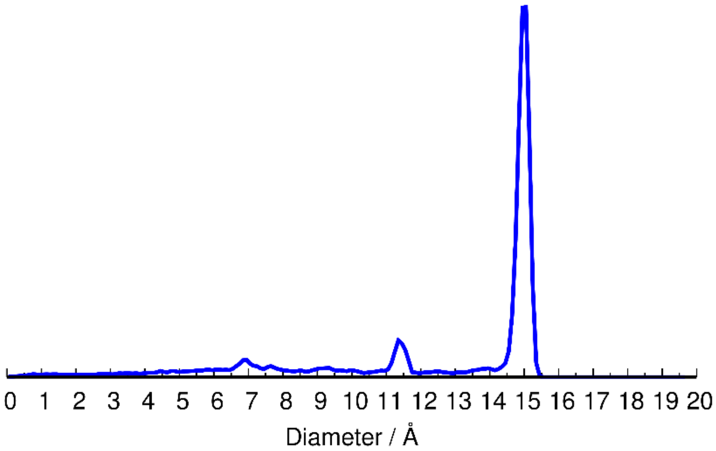

Figure S14: Pore size distribution of Cr-soc-MOF-1 calculated from the DFT optimized geometry of the solid.

NVT-MC simulations:

The DFT geometry optimized model of Cr-soc-MOF-1 was further employed in Monte Carlo (MC) calculations in the NVT ensemble loaded with the amounts of water molecules deduced from the experimental adsorption isotherms collected at $T = 298$ K and 363 K to determine the local arrangement of the adsorbed water molecules with the MOF at 298 K and 363 K using the Complex Adsorption and Diffusion Simulation Suite (CADSS) code.[17]. We considered a simulation box of 1 unit cell of Cr-soc-MOF-1 maintaining atoms at their initial positions. The water molecules were described by the TIP4P/2005 potential model corresponding to a microscopic representation of four LJ sites (see Supporting **Table S4**).[18] The interactions between the adsorbed water molecules and the MOF structure were described by a combination of site-to-site Lennard-Jones (LJ) contributions and Coulombic terms. A mixed set of the universal force field (UFF)[16] and DREIDING force field[19] parameters were adopted to describe the LJ parameters for the atoms in the inorganic and organic part of the framework, respectively (see Supporting **Table S3**). However, following the treatment adopted in other well-known force fields,[20,21] the hydrogen atoms of the water molecules coordinated to the Cr atoms of the IBUs are allowed to interact with the adsorbate water molecules via the coulombic potential only as justified in previous studies on similar Al-based MOF topologies.[22] Short-range dispersion forces were truncated at a cut-off radius of 12 Å while the interactions between unlike force field centers were treated by means of the Lorentz-Berthelot combination rule. The long-range electrostatic interactions were handled using the Ewald summation technique. For each NVT simulations, a typical 2×10^8 MC steps for equilibration and 2×10^8 MC steps have been used for production runs. Additionally, in order to gain insight into the configurational distributions of the adsorbed species in Cr-soc-MOF-1, additional data were calculated for different water loading determined at different relative pressure from the experimental volumetric adsorption isotherm, including the hydrogen bond networks and the radial distribution functions (RDF) for the intermolecular atomic pairs of the adsorbed water and the MOF.

Table S4: LJ potential parameters and partial charges for the H_2O molecules taken from TIP4P/2005 model

Atom type	**σ** [Å]	**ε/k$_B$** [K]	**q (e$^-$)**
O_e	3.1589	93.200	0.0000
H_e	0.00	0.000	0.5564
M_e	0.00	0.000	-1.1128

Hydrogen bond definition:

The detection of hydrogen bonds was conducted by assuming the following criteria: (i) distance between donor and acceptor oxygen centers (D−A) is shorter than 3.5 Å, and (ii) the corresponding D-H-A angle — formed by the intramolecular O−H vector of the donor molecule, and the intermolecular H−O vector of donor and acceptor molecules — is greater than 140°. The average number of hydrogen-bonds per H_2O was calculated from seven representative configurations taken from the MC production runs, and thereby few fluctuating data points appeared in the statistics.

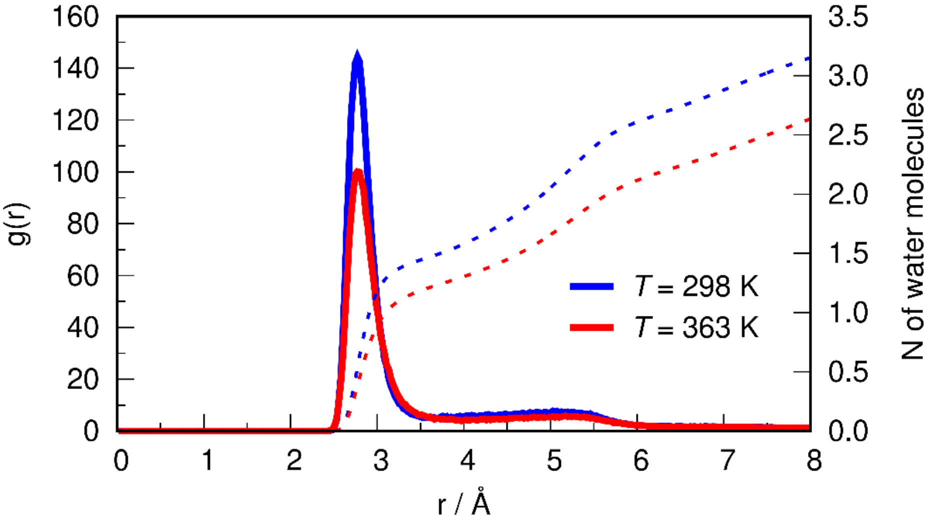

Figure S15: Radial distribution functions (RDFs) of $O_w \cdots O_w$ (solid lines) and cumulative number of water molecules as a function of the distance (dashed lines) calculated for the identical number density of adsorbed water molecules (n = 29 per unit cell) inside the MOF pore corresponding to the adsorbed water content at RH = 24.5% and 25.7 % at T = 298 K and 363 K, respectively.

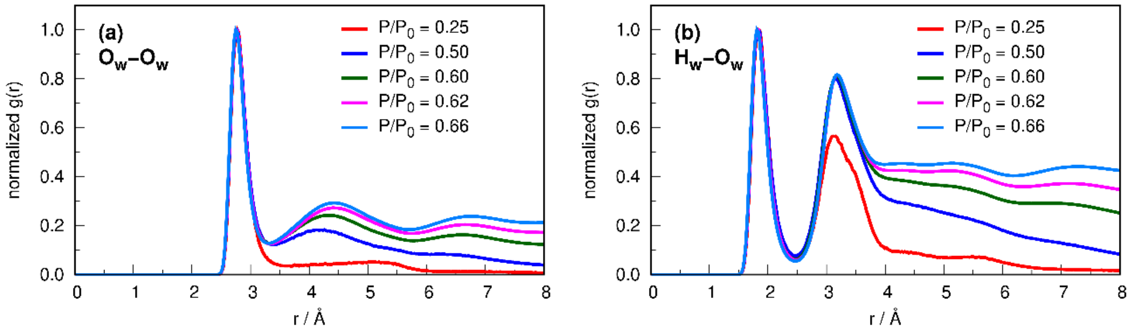

Figure S16: Radial distribution functions (RDFs) of O-O and O-H calculated from the MC-NVT simulations for different relative pressures at T = 298 K.

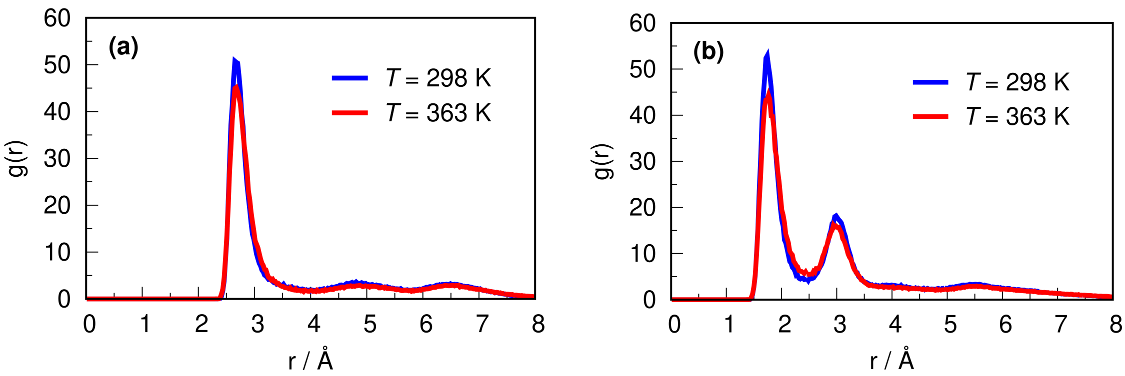

Figure S17: Radial distribution functions (RDFs) of X-O_W (**a**) and X-H_W (**b**) calculated from the MC-NVT simulations at T = 298 K and T = 363 K, with X = halogen.

References:

1 S. M. Towsif Abtab, D. Alezi, P. M. Bhatt, A. Shkurenko, Y. Belmabkhout, H. Aggarwal, Ł. J. Weseliński, N. Alsadun, U. Samin, M. N. Hedhili and M. Eddaoudi, *Chem*, 2018, **4**, 94–105.

2 P. Hohenberg and W. Kohn, *Phys. Rev.*, 1964, **136**, B864–B871.

3 W. Kohn and L. J. Sham, *Phys. Rev.*, 1965, **140**, A1133–A1138.

4 J. VandeVondele, M. Krack, F. Mohamed, M. Parrinello, T. Chassaing and J. Hutter, *Comput. Phys. Commun.*, 2005, **167**, 103–128.

5 J. Hutter, M. Iannuzzi, F. Schiffmann and J. VandeVondele, *Wiley Interdiscip. Rev. Comput. Mol. Sci.*, 2014, **4**, 15–25.

6 The CP2K developers group, http://www.cp2k.org, (accessed 10 February 2019).

7 J. P. Perdew, K. Burke and M. Ernzerhof, *Phys. Rev. Lett.*, 1996, **77**, 3865–3868.

8 S. Grimme, J. Antony, S. Ehrlich and H. Krieg, *J. Chem. Phys.*, 2010, **132**, 154104.

9 S. Grimme, *J. Comput. Chem.*, 2004, **25**, 1463–73.

10 J. VandeVondele and J. Hutter, *J. Chem. Phys.*, 2007, **127**, 114105.

11 S. Goedecker, M. Teter and J. Hutter, *Phys. Rev. B*, 1996, **54**, 1703–1710.

12 M. Krack, *Theor. Chem. Acc.*, 2005, **114**, 145–152.

13 C. Hartwigsen, S. Goedecker and J. Hutter, *Phys. Rev. B*, 1998, **58**, 3641–3662.

14 C. Campañá, B. Mussard and T. K. Woo, *J. Chem. Theory Comput.*, 2009, **5**, 2866–2878.

15 L. D. Gelb and K. E. Gubbins, *Langmuir*, 1999, **15**, 305–308.

16 A. K. Rappe, C. J. Casewit, K. S. Colwell, W. A. Goddard and W. M. Skiff, *J. Am. Chem. Soc.*, 1992, **114**, 10024–10035.

17 Q. Yang and C. Zhong, *J. Phys. Chem. B*, 2006, **110**, 655–8.

18 J. L. F. Abascal and C. Vega, *J. Chem. Phys.*, 2005, **123**, 234505.

19 S. L. Mayo, B. D. Olafson and W. A. Goddard, *J. Phys. Chem.*, 1990, **94**, 8897–8909.

20 W. L. Jorgensen, D. S. Maxwell and J. Tirado-Rives, *J. Am. Chem. Soc.*, 1996, **118**, 11225–11236.

21 C. D. Wick, J. M. Stubbs, N. Rai and J. I. Siepmann, *J. Phys. Chem. B*, 2005, **109**, 18974–18982.

22 A. Cadiau, J. S. Lee, D. Damasceno Borges, P. Fabry, T. Devic, M. T. Wharmby, C. Martineau, D. Foucher, F. Taulelle, C. H. Jun, Y. K. Hwang, N. Stock, M. F. De Lange, F. Kapteijn, J. Gascon, G. Maurin, J. S. Chang and C. Serre, *Adv. Mater.*, 2015, **27**, 4775–4780.